Specificity and affinity of the N-terminal residues in staphylocoagulase in binding to prothrombin

Received for publication, January 8, 2020, and in revised form, March 9, 2020 Published, Papers in Press, March 10, 2020, DOI 10.1074/jbc.RA120.012588

Ashoka A. Maddur[‡1], Heather K. Kroh[‡], Mary E. Aschenbrenner[‡2], Breanne H. Y. Gibson[‡], Peter Panizzi[§], Jonathan H. Sheehan[¶3], Jens Meiler[¶‖], Paul E. Bock[†‡4], and Ingrid M. Verhamme[‡4,5]

From the [‡]Department of Pathology, Microbiology, and Immunology, Vanderbilt University Medical Center, Nashville, Tennessee 37232-2561, the [§]Department of Drug Discovery and Development, Harrison School of Pharmacy, Auburn University, Auburn, Alabama 36849, the [¶]Center for Structural Biology, Vanderbilt University, Nashville, Tennessee 37232, and the [‖]Institute for Drug Discovery, Departments of Chemistry and Computer Science, Leipzig University Medical School, SAC 04103 Leipzig, Germany

Edited by Enrique M. De La Cruz

In *Staphylococcus aureus*–caused endocarditis, the pathogen secretes staphylocoagulase (SC), thereby activating human prothrombin (ProT) and evading immune clearance. A previous structural comparison of the SC(1–325) fragment bound to thrombin and its inactive precursor prethrombin 2 has indicated that SC activates ProT by inserting its N-terminal dipeptide Ile^{1}-Val^{2} into the ProT Ile^{16} pocket, forming a salt bridge with ProT's Asp^{194}, thereby stabilizing the active conformation. We hypothesized that these N-terminal SC residues modulate ProT binding and activation. Here, we generated labeled SC(1–246) as a probe for competitively defining the affinities of N-terminal SC(1–246) variants preselected by modeling. Using ProT(R155Q,R271Q,R284Q) (ProT^{QQQ}), a variant refractory to prothrombinase- or thrombin-mediated cleavage, we observed variant affinities between ~1 and 650 nM and activation potencies ranging from 1.8-fold that of WT SC(1–246) to complete loss of function. Substrate binding to ProT^{QQQ} caused allosteric tightening of the affinity of most SC(1–246) variants, consistent with zymogen activation through occupation of the specificity pocket. Conservative changes at positions 1 and 2 were well-tolerated, with Val^{1}-Val^{2}, Ile^{1}-Ala^{2}, and Leu^{1}-Val^{2} variants exhibiting ProT^{QQQ} affinity and activation potency comparable with WT SC(1–246). Weaker binding variants typically had reduced activation rates, although at near-saturating ProT^{QQQ} levels, several variants exhibited limiting rates similar to or higher than that of WT SC(1–246). The Ile^{16} pocket in ProT^{QQQ} appears to favor nonpolar, nonaromatic residues at SC positions 1 and 2. Our results suggest that SC variants other than WT Ile^{1}-Val^{2}-Thr^{3} might emerge with similar ProT-activating efficiency.

Blood clot formation by *Staphylococcus aureus* can be attributed to the combined effects of pathogen clumping and the generation of fibrin (Fbn).[6] The latter is initiated by the secreted virulence factor, staphylocoagulase (SC). Based on the bacteria's ability to promote clot formation in rabbit plasma, *S. aureus* is divided into coagulase-positive and -negative subgroups. Typing of bacterial isolates for SC is still performed today in clinical diagnosis. Coagulase-positive *S. aureus* is a potent human pathogen that causes conditions ranging from minor skin infections to life-threatening diseases, such as severe pneumonia, meningitis, and bone, joint, and heart infections. Each year ~500,000 patients in American hospitals contract staphylococcal infections that lead to ~30,000 deaths (1, 2).

Turbulent blood flow can cause endothelial damage to heart valves, exposing subendothelium that leads to deposition of platelets and Fbn. The Fbn-platelet matrix deposited on damaged valves serves as a focus for adhering *S. aureus* bacteria circulating in the blood (3). The *S. aureus*-platelet interaction is facilitated by fibrinogen (Fbg), fibronectin, thrombospondin, and MSCRAMMs (microbial surface components recognizing adhesive matrix molecules), such as protein A and Fbg-binding ClfA (clumping factor A) (4–11). In acute bacterial endocarditis, Fbn formation is mediated by the thrombin precursor prothrombin (ProT), conformationally activated by bacterial SC. This furthers aggregation of platelets and enlargement of platelet-Fbn-bacteria vegetations on the valves (3). These friable vegetations can break up and cause pulmonary embolism and stroke. The pathogens also utilize these vegetations to disseminate and avert clearance by the host immune system (12).

This research was supported in part by National Institutes of Health Grants R01 HL071544 (to P. E. B. and I. M. V.), R01 HL114477 (to P. P.), and R01 HL122010 (to Alfred George, providing support for J. M.). The authors declare that they have no conflicts of interest with the contents of this article. The content is solely the responsibility of the authors and does not necessarily represent the official views of the National Institutes of Health.
This article contains Tables S1 and S2 and Fig. S1.

† Deceased.

[1] To whom correspondence may be addressed: Dept. of Pathology, Microbiology, and Immunology, Vanderbilt University Medical Center, C3321A Medical Center North, Nashville, TN 37232-2561. Tel.: 615-343-9863; Fax: 615-343-7023; E-mail: ashoka.maddur@vumc.org.
[2] Present address: Duke University Medical Center, 2301 Erwin Rd., Durham, NC 27710.
[3] Present address: Dept. of Medicine, Infectious Diseases Division, Washington University School of Medicine, 660 South Euclid, St. Louis, MO 63110.
[4] Senior co-authors.
[5] To whom correspondence may be addressed: Dept. of Pathology, Microbiology, and Immunology, Vanderbilt University Medical Center, C3321A Medical Center North, Nashville, TN 37232-2561. Tel.: 615-343-9863; Fax: 615-343-7023; E-mail: ingrid.verhamme@vanderbilt.edu.

[6] The abbreviations used are: Fbn, fibrin; SC, staphylocoagulase; SC(1–246)-BODIPY, SC(1–246)-S7C-BODIPY-FL; Fbg, fibrinogen; ProT, prothrombin; ProT^{QQQ}, prothrombin mutant with mutations at arginines 155, 271, and 284 substituted to glutamine; Pre2, prethrombin 2; vWbp, von Willebrand factor–binding protein; REU, Rosetta energy unit(s); PTI, pancreatic trypsin inhibitor; pGB, *p*-guanidinobenzoate; V_{lim}, limiting velocity.

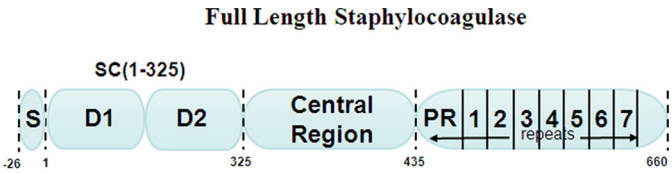

Figure 1. Full-length staphylocoagulase from *S. aureus* Newman D2 Tager 104 showing different regions of the protein. The full-length protein contains a 26-residue signal sequence, the D1 and D2 domains, a central region, and a C-terminal repeat region consisting of a pseudo-repeat (*PR*) and seven repeats.

Acute bacterial endocarditis caused by *S. aureus* leads to 20–40% mortality despite antibiotic therapy (13).

Blood clotting is a highly regulated process, with a delicate balance between clotting and fibrinolysis. SC bypasses the clotting cascade by directly and nonproteolytically activating ProT, thereby shifting the balance to a procoagulant state. SC binds and conformationally activates ProT, forming a complex of catalytically active zymogen and activator, SC·ProT* (with the asterisk denoting a functional catalytic site). The activated complex cleaves Fbg to form Fbn clots involved in enlarging the vegetations. No physiological inhibitors of the SC·ProT* complex have been reported to date, and it is resistant to the plasma serpins, antithrombin-heparin and heparin cofactor II,[7] α2-macroglobulin (14), and the leech inhibitor, hirudin (15).

SC is a bifunctional protein with a molecular mass of ~75,000 Da. Its N-terminal region binds ProT (16), whereas the C-terminal region contains seven 27-amino acid-repeat sequences that bind Fbg (Fig. 1) (17, 18). We previously described that the SC fragment consisting of N-terminal residues 1–325, SC(1–325), binds ProT extremely tightly (~17–72 pM) and noncovalently in a 1:1 stoichiometry to form the active SC(1–325)·ProT* complex (19). A comparison of the crystal structures of SC(1–325) with thrombin and the inactive zymogen prethrombin 2 (Pre2, prothrombin without the fragments 1 and 2) showed that the first six residues of the SC fragment were fully defined by electron density in the complex with Pre2 but not with thrombin. SC activates the zymogen by inserting its N-terminal Ile^1-Val^2 (I1V2 amino acid single-letter code) residues into the Ile^{16} pocket of Pre2, forming a salt bridge with Asp^{194} and inducing a functional active site in the zymogen (19). Formation of the SC(1–325)·ProT* and SC(1–325)·Pre2* complexes partially blocks exosite 1, the Fbg-binding site, but expresses a new Fbg substrate recognition site that facilitates Fbg binding and cleavage (Fig. 2). SC(1–325) consists of two three-helix-bundle domains (D1 (residues 1–146) and D2 (residues 147–325)) with a boomerang-like structure. The D1 domain interacts with the 148-loop of thrombin or Pre2 and the south rim of the catalytic site, and the D2 domain binds (pro)-exosite 1 on Pre2 and thrombin. We report here that SC(1–246), with a partially truncated D2 domain, is capable of ProT activation and binds ProT with a K_D of ~1 nM, which made it a suitable probe for determining the affinities of mutant SC constructs by competitive equilibrium binding. The I1V2 residues are critically involved in SC-mediated ProT activation, and a comparison of the SC N-terminal residues from 12 different

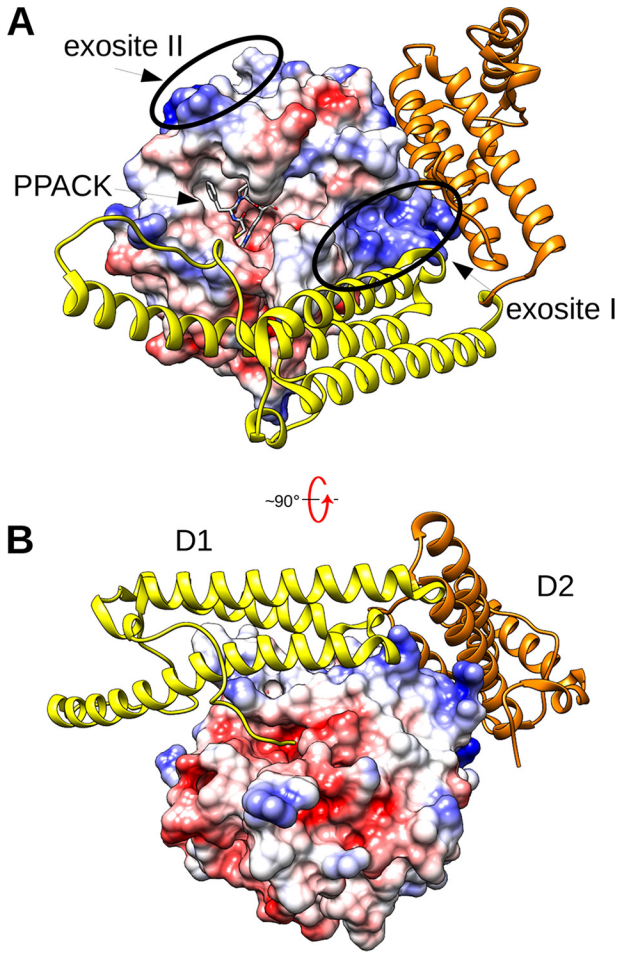

Figure 2. The SC(1–325)·Pre2 complex. *A*, the molecular surface of Pre2 is shown *colored* by electrostatic potential, with the ATA-PPACK (*N*-(sulfanylacetyl)-D-phenylalanyl-*N*-[(2S,3S)-6-{[amino(iminio)methyl]amino}-1-chloro-2-hydroxyhexan-3-yl]-L-prolinamide) inhibitor displayed as *gray sticks* in the active site. SC(1–325) is displayed in *ribbon mode*, with the N-terminal D1 domain *colored yellow* and the D2 domain *colored gold*. *B*, the complex above is rotated ~90° from the standard orientation to show the insertion of the N-terminal SC peptide Ile^1-Val^2-Thr^3 into the Ile^{16}-binding pocket of Pre2, triggering activation. This figure was constructed with UCSF Chimera using the X-ray crystal structure 1NU9.pdb (16).

S. aureus strains showed strict conservation of I1V2T3. This raised the question of whether *S. aureus* could possibly make SC mutants that contain N-terminal residues different from I1V2T3 and what the effect of these other N-terminal residues on the affinity and activation of ProT might be. Because 8,000 different combinations are possible, our selection was guided by *in silico* protein modeling with Rosetta and virtual screening to prioritize combinations with high binding free energy and to identify a range of affinities and activation potencies. In this study, 46 different N-terminal mutants of SC(1–246) were generated through site-directed mutagenesis and characterized for binding and activation of a ProT(R155Q,R271Q,R284Q) mutant ($ProT^{QQQ}$) that can be proteolytically activated to a meizothrombin form refractory to cleavage by prothrombinase and thrombin (20) but was used in this study to monitor conformational activation of prothrombin instead of proteolytic activation. The panel displayed a wide range of activation potencies and K_D values both by equilibrium binding and $ProT^{QQQ}$ activation. The V1V2, I1A2, and L1V2 mutants bound

[7] I. M. Verhamme, P. Panizzi, and P. E. Bock, unpublished observations.

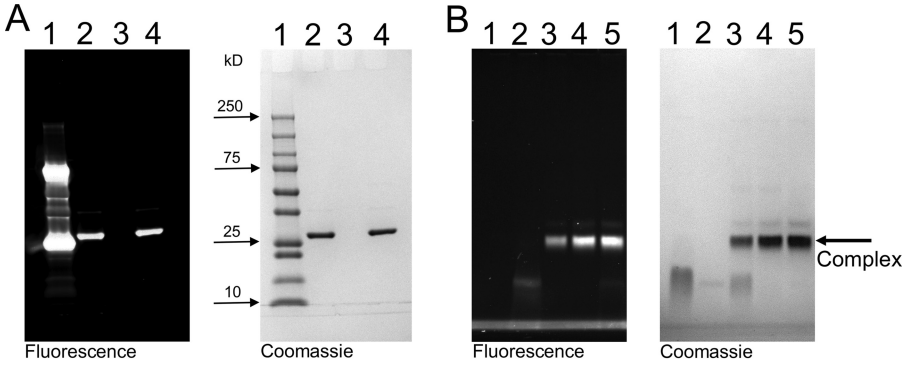

Figure 3. Characterization of SC(1–246)-BODIPY and its complex with ProT^{QQQ}. *A*, SDS-PAGE showing the purity of the labeled probe, SC(1–246)-BODIPY. 5 μg of the labeled probe was separated under reduced (*lane 2*) and nonreduced (*lane 4*) conditions. *Lane 1*, protein standards; *lane 3*, blank. *B*, native gel electrophoresis was used to show the SC(1–246)-BODIPY·ProT^{QQQ} complex formation. ProT^{QQQ} (2.5 μM, *lane 1*) was incubated with SC(1–246)-BODIPY (0-fold (*lane 2*), 0.5-fold (*lane 3*), 1.0-fold (*lane 4*), and 1.5-fold (*lane 5*) excess of ProT^{QQQ}) for 15–30 min at 25 °C, and the complex was separated on native PAGE at 4 °C.

ProT^{QQQ} with affinities similar to that of WT SC(1–246) and with ProT^{QQQ} activation potencies that were similar or up to 1.8-fold greater. Activation potencies of mutants with both weak equilibrium binding and activation-based affinities were typically reduced. Select mutants carrying nonpolar residues at position 1 bound moderately to ProT^{QQQ} when measured by equilibrium binding but exhibited tight (approximately nanomolar) binding when measured by ProT^{QQQ} activation, indicating a difference in affinity when binding to a disordered Ile^{16} pocket (equilibrium binding) and an Ile^{16} pocket conformationally stabilized by substrate occupation of the specificity site. These mutants had limiting activation rates similar to or exceeding that of WT SC(1–246). Overall, the Ile^{16} pocket of ProT^{QQQ} favors nonpolar, nonaromatic residues at positions 1 and 2, however with specific restrictions governed by steric complementarity between the N terminus of SC and the Ile^{16} pocket of ProT. Our results, including efficient activation of ProT by weaker binding mutants at saturating concentrations, suggest that SC variants might emerge with similar or higher efficiency to activate ProT.

Results

Characterization of SC(1–246)-BODIPY and equilibrium binding of labeled and unlabeled SC(1–246) to ProT^{QQQ}

SC(1–246)-BODIPY had a labeling ratio of 0.87 BODIPY-FL thiol-sensitive probe to SC(1–246) with a S7C substitution for covalent probe binding (Fig. 3*A*). Incubation of ProT^{QQQ} with SC(1–246)-BODIPY showed binding in an approximately 1:1 ratio as observed by native PAGE (Fig. 3*B*). Competitive equilibrium binding studies were performed to determine the affinity and stoichiometry of four separate ProT^{QQQ} preparations for unlabeled SC(1–246) and SC(1–246)-BODIPY. Unlabeled SC(1–246) bound very tightly to the ProT^{QQQ} preparations, with K_D of 0.6–1.0 nM, and a 1:1 stoichiometry (Fig. 4 and Table 1). SC(1–246)-BODIPY bound ProT^{QQQ} with K_D of 2.9–5.9 nM and a stoichiometry of 1:1. This weaker affinity is attributed to the BODIPY-FL label. Batch-to-batch variability of ProT^{QQQ} was modest, as reflected by the consistent affinity values for unlabeled and labeled SC(1–246). The maximum fluorescence intensity was 0.6 ± 0.1 for all of the ProT^{QQQ} preparations.

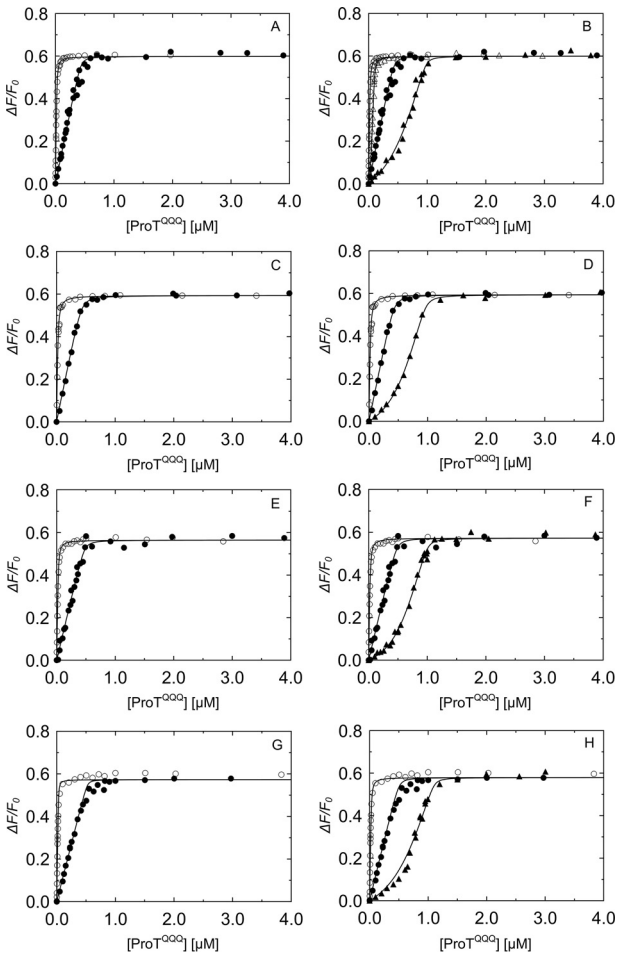

Figure 4. Equilibrium binding of SC(1–246)-BODIPY and WT SC(1–246) to ProT^{QQQ}. *A*, *C*, *E*, and *G*, SC(1–246)-BODIPY (29 nM (○) and 502 nM (●)) titrated with ProT^{QQQ}, four separate batches. *B*, titration of 29 nM SC(1–246)-BODIPY (○); a mixture of 50 nM SC(1–246)-BODIPY and 50 nM WT SC(1–246) (△); 502 nM SC(1–246)-BODIPY (●); and a mixture of 502 nM SC(1–246)-BODIPY and 500 nM WT SC(1–246) (▲) with ProT^{QQQ}. *D*, *F*, and *H*, titrations of SC(1–246)-BODIPY (29 nM (○) and 502 nM (●)) and a mixture of 502 nM SC(1–246)-BODIPY and 500 nM WT SC(1–246) (▲) with ProT^{QQQ}. Titrations shown in *B*, *D*, *F*, and *H* were performed with the corresponding, separate ProT^{QQQ} preparations as in *A*, *C*, *E*, and *G*. The SC(1–246)-BODIPY titration data were analyzed by the quadratic binding equation to obtain the affinity, stoichiometry, and maximum fluorescence intensity ($\Delta F_{max}/F_o$). Titration data of the probe and competitor were analyzed simultaneously by the cubic binding equation to obtain the affinity and stoichiometry of the competitor, WT SC(1–246) (Table 1).

Table 1

Parameters for SC(1–246)-BODIPY and unlabeled WT SC(1–246) binding to four separate ProT^{QQQ} preparations

Reference titrations of SC(1–246)-BODIPY with four separate ProT^{QQQ} batches were obtained at two fixed probe concentrations. The competitive binding data for the ProT^{QQQ} preparations were obtained by titrations of fixed concentrations of SC(1–246)-BODIPY probe, and SC(1–246) as competitor, with ProT^{QQQ}. Data were fit simultaneously by the cubic equation to obtain the dissociation constant for ProT^{QQQ} and SC(1–246)-BODIPY (K_O, probe) and the competitor SC(1–246) (K_C, competitor); the stoichiometric factor for SC(1–246)-BODIPY (n) and SC(1–246) (m); and the maximum fluorescence intensity ($\Delta F_{max}/F_o$). Experimental error represents ± 2 S.D. Competitive equilibrium binding studies and data analysis were performed as described under "Experimental procedures." SF, stoichiometric factor.

SC(1–246)	SF (n or m)	K_O or K_C	$\Delta F_{max}/F_o$
		nM	
SC(1–246)-BODIPY (n)	0.90 ± 0.03	2.9 ± 0.7	0.60 ± 0.01
SC(1–246) (m)	1.10 ± 0.05	0.7 ± 0.2	
SC(1–246)-BODIPY (n)	0.90 ± 0.02	5.9 ± 0.8	0.59 ± 0.01
SC(1–246) (m)	1.10 ± 0.06	1.0 ± 0.3	
SC(1–246)-BODIPY (n)	1.00 ± 0.04	4.1 ± 1.1	0.57 ± 0.01
SC(1–246) (m)	1.10 ± 0.05	0.7 ± 0.2	
SC(1–246)-BODIPY (n)	1.01 ± 0.06	3.0 ± 1.4	0.58 ± 0.01
SC(1–246) (m)	1.20 ± 0.08	0.6 ± 0.4	

Binding prediction and competitive equilibrium binding of SC(1–246) N-terminal mutants to ProT^{QQQ}

Computational modeling used Rosetta's ΔΔG functionality to calculate the predicted change in binding energy for each mutation (21), sampling all 20 amino acids at positions 1–3. The fixed backbone design strategy allowed discrimination between steric clashing and nonclashing sequences, and based on the resulting energies in Rosetta energy units (REU), a representative double and triple N-terminal mutant panel was selected for experimental binding studies, with expected K_D values between 1 and ~1000 nM. Equilibrium binding showed that the double mutants V1V2, I1A2, and L1V2 bound to ProT^{QQQ} very tightly, with affinities of ~1 nM, similar to that of WT SC(1–246) (Fig. 5, *A–C*). Their excellent ProT^{QQQ} activation potency also indicated efficient salt bridge formation with ProT^{QQQ} Asp^{194} and formation of the ProT^{QQQ} active site. The stoichiometric factor was ~1, indicating that 1 mol of ProT^{QQQ} binds to 1 mol of SC(1–246) mutant. The K_D values from equilibrium binding were measured in the absence of a conformationally stabilizing tripeptide thrombin substrate, and they reflect global binding to ProT^{QQQ} with a disordered Ile^{16} pocket and specificity subsite. The V1V2, I1A2, and L1V2 combinations of nonpolar residues had comparable equilibrium binding and activation K_D values, suggesting a favorable steric complementarity to the Ile^{16} pocket. Mutants with weaker equilibrium K_D values may be governed mainly by the D1 and truncated D2 domain interactions with ProT^{QQQ}, although double mutants with Ile, Val, Leu, and Thr in combination with polar, nonpolar aromatic, bulky, or small residues at position 2 exhibited considerable tightening of the binding to ProT^{QQQ} when an Ile^{16} pocket-stabilizing substrate was present (Fig. 5 and Tables 2 and 3). The A1S2 and A1T2 mutants exhibited weak equilibrium binding affinity; however, the presence of a chromogenic substrate during ProT^{QQQ} activation caused these mutants to bind with ~30–100-fold tighter K_D, respectively, and exhibit WT-like activation potency. This suggests some conformational flexibility of the ordered Ile^{16} pocket. Mutants with charged residues (Lys, Arg, Asp, Glu, His) in positions 1 and/or 2; Gly or Trp in position 1; or Pro in position 2 typically bound weakly and were poor activators, with G1G2 the weakest binder (Fig. 6 and Tables 2 and 3). Although disrupted binding for Pro was expected, even some pairs with small, hydrophobic residues in positions 1 and 2 may not optimally fit, illustrating the steric specificity of the Ile^{16}-binding pocket.

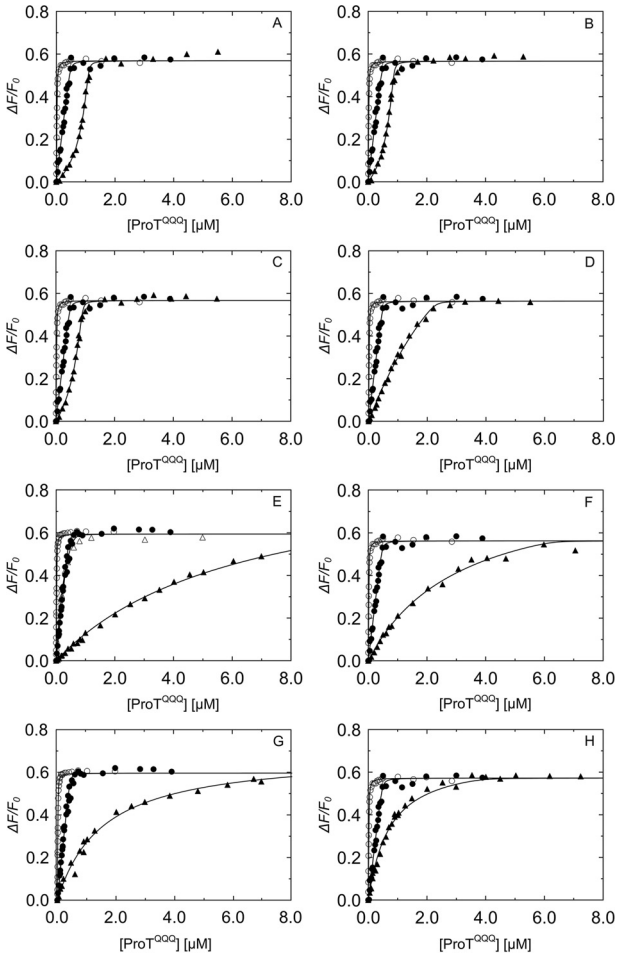

Figure 5. Competitive binding of SC(1–246) N-terminal double mutants that bind tightly to ProT^{QQQ}. Titrations of the probe, SC(1–246)-BODIPY (29 nM (○) and 502 nM (●)), with ProT^{QQQ} from Fig. 4 served as reference curves for competitive titrations of SC(1–246) mutants. The probe concentration for all of the competitive titrations (△, ▲) in *A–H* was 50 nM. Concentrations of competing SC(1–246) mutants were as follows: V1V2 0.90 μM (*A*), I1A2 0.74 μM (*B*), L1V2 0.75 μM (*C*), I1T2 2.24 μM (*D*), I1W2 0.52 μM (△) and 9.97 μM (▲) (*E*), T1V2 6.16 μM (*F*), L1T2 9.55 μM (*G*), and L1Q2 3.95 μM (*H*). Titrations of probe and competitor were simultaneously analyzed by the cubic binding equation to obtain K_C, stoichiometry, and maximum fluorescence intensity ($\Delta F_{max}/F_o$) of the SC(1–246) mutants (Tables 2 and 3).

Equilibrium binding K_D values of triple mutants varied from ~4 to ~55 nM (Table 4). The mutant I1I2V3 bound ProT^{QQQ} with a K_D of 4 ± 3 nM (Fig. 7*A*) and activated ProT^{QQQ} at an appreciable rate, suggesting that the ProT^{QQQ} Ile^{16} pocket accommodates these nonpolar residues with reasonable fit, conducive to forming a salt bridge with ProT^{QQQ} Asp^{194}. The mutants R1H2W3, F1L2Q3, E1S2W3, D1D2Y3, G1G2G3, and E1L2K3 had K_D values of 36–55 nM (Fig. 7, *B–G*) but activated ProT^{QQQ} poorly. Interestingly, substituting Gly^3 for WT Thr^3 rescued equilibrium binding ~10-fold, compared with G1G2, but with no improvement in activation potency.

Table 2
Characteristics of N-terminal residues in relation to mutant SC(1–246) affinity and ProT^{QQQ} activation potency

N-terminal mutants	Residue 1 characteristics	Residue 2 characteristics	Affinity range (K_D)	Activation potency normalized (V_{lim})	Free energy (ΔG)
			nM		
I1V2 WT	Nonpolar	Nonpolar	0.7 ± 0.2	1.0	−12.48
V1V2, I1A2, and L1V2	Similar nonpolar	Similar nonpolar	~0.9–1.3	~1.0–1.80	− 12.33 to − 12.11
I1T2, I1W2, I1L2, and V1G2	Similar nonpolar	Polar, nonpolar, indole	~5–100	~0.9–1.60	− 11.29 to − 9.55
T1V2, T1P2, and T1A2	Polar	Nonpolar, pyrrolidine	~11–100	~0.4–1.70	− 10.88 to − 9.55
L1T2, L1Q2, L1K2, and L1P2	Similar nonpolar	Nonpolar, pyrrolidine, charged	~19–220	~0.3–1.6	− 10.54 to − 9.08
W1A2 and W1E2	Indole	Nonpolar, charged	~117–191	ND[a]	− 9.45 to − 9.17
M1L2, M1W2, M1K2, and M1E2	Bulky nonpolar	Nonpolar, indole, charged	~127–514	~0.06–1.1	− 9.40 to − 8.58
G1H2, G1A2, G1P2, G1D2, G1G2, A1W2, A1K2, A1S2, and A1T2	Small nonpolar	Small nonpolar, polar, charged, aromatic	~153–503	~0.02–1.0	− 9.29 to − 8.62
Q1K2, T1D2, S1K2, Q1L2, and N1D2	Polar	Charged, nonpolar	~169–493	~0.02–0.24	− 9.24 to − 8.58
R1R2, K1A2, E1T2, R1Q2, and E1S2	Charged	Charged, nonpolar, polar	~379–650	~0.004–0.1	− 8.76 to − 8.44

[a] ND, not determined.

Table 3
ProT^{QQQ} binding and activation by SC(1–246) N-terminal double mutants

Reference titrations of SC(1–246)-BODIPY with ProT^{QQQ} were obtained at two fixed probe concentrations. Competitive binding data were obtained by titrations of fixed concentrations of SC(1–246)-BODIPY probe, and mutant SC(1–246) as competitor, with ProT^{QQQ}. Data were fit simultaneously by the cubic equation to obtain the dissociation constant for ProT^{QQQ} and SC(1–246)-BODIPY (K_D, *probe*) and mutant SC(1–246) (K_D, *competitor*); the stoichiometric factor for SC(1–246)-BODIPY (*n*) and mutant SC(1–246) (*m*); and the maximum fluorescence intensity ($\Delta F_{max}/F_o$). Experimental error represents ± 2 S.D. Competitive equilibrium binding studies and data analysis were performed as described under "Experimental procedures." ND, not determined; SF, stoichiometric factor.

SC(1–246) mutants	SF (*m*)	*KC*	$\Delta F_{max}/Fo$	ΔG	K_D from ProT^{QQQ} activation	V_{lim}	*REU* complex (predicted)
	mol ProT^{QQQ}/mol SC (1–246)	*nM*		*kcal/mol*	*nM*		*REU*
I1V2	1.10 ± 0.05	0.7 ± 0.2	0.60 ± 0.01	−12.48	1.5 ± 0.2	1.0 ± 0.01	−130
V1V2	1.17 ± 0.04	0.9 ± 0.3	0.60 ± 0.05	−12.33	2.1 ± 0.5	1.0 ± 0.01	−128
I1A2	1.13 ± 0.02	1.1 ± 0.3	0.57 ± 0.01	−12.25	4.2 ± 0.5	1.8 ± 0.01	−126
L1V2	1.14 ± 0.04	1.3 ± 0.4	0.57 ± 0.004	−12.11	4.1 ± 1.0	1.4 ± 0.1	−117
I1T2	1.01 ± 0.09	5.3 ± 1.7	0.56 ± 0.01	−11.29	5.0 ± 1.4	0.90 ± 0.08	−125
I1W2	1.13 ± 0.12	7.1 ± 2.4	0.59 ± 0.01	−11.11	1.8 ± 0.2	0.92 ± 0.01	481
T1V2	1.02 ± 0.16	11 ± 4	0.56 ± 0.01	−10.88	8 ± 2	1.7 ± 0.1	−124
L1T2	Fixed to 1	19 ± 6	0.60 ± 0.01	−10.54	3.0 ± 0.4	1.4 ± 0.1	−112
L1Q2	Fixed to 1	27 ± 7	0.57 ± 0.01	−10.33	1.2 ± 0.4	1.3 ± 0.1	−108
T1P2	Fixed to 1	61 ± 40	0.57 ± 0.01	−9.84	169 ± 34	0.38 ± 0.03	−57
I1L2	Fixed to 1	64 ± 17	0.57 ± 0.01	−9.82	7 ± 1	1.3 ± 0.1	−119
L1K2	Fixed to 1	76 ± 12	0.60 ± 0.01	−9.71	3.0 ± 0.3	1.6 ± 0.1	−110
V1G2	Fixed to 1	100 ± 27	0.60 ± 0.01	−9.55	3.1 ± 0.4	1.6 ± 0.1	−122
T1A2	Fixed to 1	100 ± 27	0.60 ± 0.01	−9.55	5.2 ± 0.2	1.3 ± 0.1	−120
W1A2	Fixed to 1	117 ± 36	0.60 ± 0.01	−9.45	ND	ND	1,298
M1L2	Fixed to 1	127 ± 38	0.58 ± 0.01	−9.41	16 ± 2	0.90 ± 0.02	−107
M1W2	Fixed to 1	148 ± 27	0.60 ± 0.01	−9.32	8 ± 1	0.25 ± 0.01	493
G1H2	Fixed to 1	153 ± 43	0.61 ± 0.01	−9.29	346 ± 134	0.02 ± 0.003	−115
G1A2	Fixed to 1	166 ± 42	0.60 ± 0.01	−9.25	46 ± 5	0.17 ± 0.01	−118
Q1K2	Fixed to 1	169 ± 49	0.60 ± 0.01	−9.24	59 ± 8	0.20 ± 0.01	−116
A1W2	Fixed to 1	170 ± 60	0.58 ± 0.01	−9.23	44 ± 5	0.14 ± 0.01	487
M1K2	Fixed to 1	174 ± 54	0.58 ± 0.01	−9.22	9 ± 1	1.1 ± 0.1	−111
W1E2	Fixed to 1	191 ± 54	0.60 ± 0.01	−9.17	5,700 ± 4,200	0.13 ± 0.06	1,307
A1K2	Fixed to 1	191 ± 62	0.58 ± 0.01	−9.16	27 ± 2	0.55 ± 0.11	−116
L1P2	Fixed to 1	220 ± 64	0.58 ± 0.01	−9.08	22 ± 3	0.31 ± 0.01	−50
T1D2	Fixed to 1	248 ± 72	0.58 ± 0.01	−9.01	100 ± 18	~0.2	−115
S1K2	Fixed to 1	251 ± 76	0.58 ± 0.01	−9	44 ± 2	0.16 ± 0.01	−115
Q1L2	Fixed to 1	277 ± 83	0.58 ± 0.01	−8.94	188 ± 21	0.024 ± 0.001	−111
A1S2	Fixed to 1	295 ± 69	0.60 ± 0.01	−8.91	11 ± 0.4	1.0 ± 0.1	−118
R1R2	Fixed to 1	379 ± 88	0.61 ± 0.01	−8.76	26 ± 5	0.1 ± 0.01	−104
G1P2	Fixed to 1	446 ± 81	0.61 ± 0.01	−8.66	64 ± 6	0.020 ± 0.001	−54
K1A2	Fixed to 1	455 ± 80	0.60 ± 0.01	−8.65	69 ± 20	0.010 ± 0.001	−111
G1D2	Fixed to 1	468 ± 80	0.61 ± 0.01	−8.63	76 ± 7	0.020 ± 0.001	−113
A1T2	Fixed to 1	480 ± 95	0.60 ± 0.01	−8.62	5 ± 0.3	1.0 ± 0.1	−118
E1T2	Fixed to 1	486 ± 80	0.60 ± 0.01	−8.61	105 ± 11	0.030 ± 0.001	−113
N1D2	Fixed to 1	493 ± 99	0.60 ± 0.01	−8.6	89 ± 7	0.020 ± 0.001	−113
G1G2	Fixed to 1	503 ± 90	0.61 ± 0.01	−8.59	26 ± 2	0.26 ± 0.01	−115
R1Q2	Fixed to 1	503 ± 94	0.60 ± 0.01	−8.59	35 ± 26	0.004 ± 0.010	−104
M1E2	Fixed to 1	514 ± 96	0.60 ± 0.01	−8.58	56 ± 8	0.060 ± 0.001	−105
E1S2	Fixed to 1	650 ± 120	0.61 ± 0.01	−8.44	205 ± 14	0.010 ± 0.002	−112

The Gibbs free energy ΔG for binding of the mutants varied from −12.45 to −8.44 kcal/mol (Tables 2–4 and Fig. 8), with the lowest value for WT SC(1–246), calculated from the averaged K_D for binding to the four ProT^{QQQ} batches. V1V2, I1A2, L1V2, I1T2, I1W2, and I1I2V3 had ΔG values similar to the WT protein, consistent with K_D values in the nanomolar range. A good correlation was observed between the predicted Rosetta energies and the ΔG values calculated from equilibrium binding (Fig. 9), except for a few outliers (T1P2, W1A2, M1W2, A1W2, W1E2, L1P2, and G1P2) that gave inconsistent Rosetta energies but also exhibited reduced activation potency (Fig. S1). These outliers occur in the presence of Pro^2 and of Trp^1 or Trp^2 and display an off-scale energetic prediction because Rosetta is unable to fit them into the structure of the complex. This is not unexpected behavior; the introduction of a Pro or Trp residue may require such major conformational rearrangement, due to

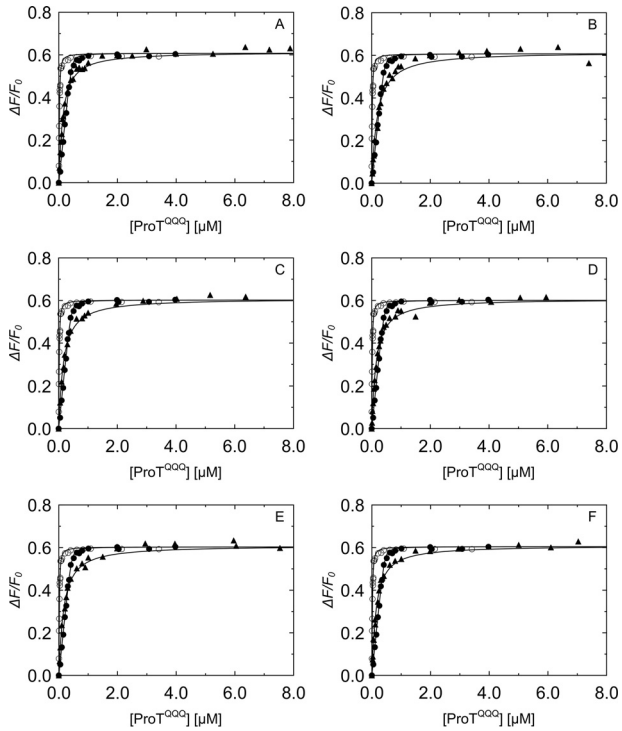

Figure 6. Competitive binding titrations of SC(1–246) N-terminal double mutants that bind weakly to ProT^{QQQ}. Titrations of the probe, SC(1–246)-BODIPY (29 nM (○) and 502 nM (●)) with ProT^{QQQ} from Fig. 4 served as reference curves for competitive titrations of SC(1–246) mutants. The probe concentration for all of the competitive titrations (▲) in *A–F* was 50 nM. Concentrations of competing SC(1–246) mutants were as follows: G1G2 8.12 μM (*A*), R1R2 9.06 μM (*B*), K1A2 9.50 μM (*C*), E1T2 9.04 μM (*D*), R1Q2 10.30 μM (*E*), and E1S2 11.38 μM (*F*). Titrations of probe and competitor were simultaneously analyzed by the cubic binding equation to obtain K_C, stoichiometry, and maximum fluorescence intensity ($\Delta F_{max}/F_o$) of the SC(1–246) mutants (Tables 2 and 3).

steric clash or backbone geometry restriction, that the score penalty increases beyond the ability of the sampling protocol to incorporate it. Additional sampling might be necessary to create accurate models for these large or conformationally restricted amino acids. The only unexpected discrepancy was I1W2 with an REU score of 481 but exhibiting WT-like binding and ProT^{QQQ} activation properties. The behavior of I1W2 is difficult to rationalize; the high Rosetta score reflects our expectation that inserting the steric bulk of a Trp residue at position 2 would be unfavorable. This prediction is consistent with the predictions and measurements of other mutants containing Trp at position 2. We can only conjecture that the I1W2 combination permits binding and activation via an unknown mechanism.

Prothrombin activation by SC(1–246) N-terminal double and triple mutants

Initial rates v_0 of *p*-nitroanilide formation upon chromogenic substrate cleavage by the ProT^{QQQ}·SC complexes were linear for WT SC(1–246) and tight-binding mutants, and the titrations showed saturation around 20 nM SC(1–246) variant. A few mutants caused hysteresis-like lag phases in substrate hydrolysis by their complexes with ProT^{QQQ}, and post-lag, linear v_0 rates were used for analysis of these mutants. The limiting velocity (V_{lim}) of WT SC(1–246) was 20 ± 5 mAbs/min, in good agreement for all four ProT^{QQQ} batches, and used as the 100% value, or 1.00, for normalizing assays of slow-activating mutants to 1 nM ProT^{QQQ}. K_D and V_{lim} values derived from the ProT^{QQQ} activation analysis are given in Table 3. The V1V2, I1A2, and L1V2 mutants with affinities similar to WT SC(1–246) activated ProT^{QQQ} with similar or higher potency than WT SC(1–246). I1A2 and L1V2 showed ~81 and ~41% increase in ProT^{QQQ} activity, suggesting that Ala^2 and Leu^1 nonpolar residues bound tightly and fit optimally in the Ile^{16} pocket of ProT^{QQQ} for Ile^1 and Leu^1 bonding with Asp^{194}, resulting in increased ProT^{QQQ} activity. Apparent K_D values for these tight-binding mutants, derived from the activation kinetics, were in good agreement with those measured by equilibrium binding (Fig. 10). Most mutants with a weaker equilibrium binding K_D for ProT^{QQQ} also activated ProT^{QQQ} weakly, with relative $V_{lim} \ll 1$, although some, like M1L2, A1T2, A1S2, M1K2, T1A2, L1Q2, I1L2, L1T2, L1K2, V1G2, and T1V2 activated ProT^{QQQ} similarly or up to 1.7-fold better than WT SC(1–246) at mutant concentrations approaching ProT^{QQQ} saturation with regard to K_D calculated from the activation profiles (Tables 2–4). The affinities of these mutants, defined by ProT^{QQQ} activation, were typically higher than their counterparts defined by equilibrium binding, due to allosteric modulation of the binding by the presence of the chromogenic substrate occupying the specificity pocket of the zymogen. This was previously also reported for vWbp binding to FPR derivatives of prothrombin, prethrombin 1 and 2 (22), and the binding of oligopeptides to trypsinogen with the specificity site occupied by a covalent ligand or a tight-binding inhibitor (23). Affinities defined for triple mutants that activated ProT^{QQQ} poorly were not well-defined due to large experimental error. Overall, nonpolar hydrophobic residues were well-tolerated in position 1, whereas polar, aromatic, or charged residues generally diminished the ProT^{QQQ} activation potency. Due to its conformational rigidity and unusual configuration, Pro in position 2 is thought to hamper efficient salt bridge formation of any residue at position 1, with a greatly diminished activation potency as a result.

Discussion

In physiological blood coagulation, ProT is proteolytically cleaved in a multistep process to form the central clotting protease, thrombin (24). Proteolytic activation of ProT and Pre2 is initiated by cleavage of the peptide bond between Arg^{15} and Ile^{16} (chymotrypsinogen numbering). The newly formed I1V2 N terminus inserts into the Ile^{16} pocket of the zymogen, triggering the folding of zymogen activation domain residues 142–152, 186–194, and 216–226, and the α-ammonium of group of Ile^1 forms a salt bridge with the carboxylate of Asp^{194}. This generates the substrate recognition subsites and the oxyanion hole (25, 26). In contrast, SC, a virulence factor secreted by *S. aureus*, is a potent nonproteolytic ProT activator. Our structure-function studies on SC constructs in complex with ProT, Pre2, and thrombin demonstrate that the SC I1V2 residues are critical for ProT and Pre2 activation. As shown in the crystal structure of the SC(1–325)·Pre2 complex, these residues insert into the Ile^{16} pocket of Pre2, with SC Ile^1 forming the salt bridge with Asp^{194}, and conformational changes resulting in the gen-

Table 4

ProT^{QQQ} binding and activation by SC(1–246) N-terminal triple mutants

Reference titrations of SC(1–246)-BODIPY with ProT^{QQQ} were obtained at two fixed probe concentrations. The competitive binding data were obtained by titrations of fixed concentrations of SC(1–246)-BODIPY probe, and triple mutant SC(1–246) as competitor, with ProT^{QQQ}. Data were fit simultaneously by the cubic equation to obtain the dissociation constant for ProT^{QQQ} and SC(1–246)-BODIPY (K_O, probe) and mutant SC(1–246) (K_C, competitor); the stoichiometric factor for SC(1–246)-BODIPY (n) and mutant SC(1–246) (m); and the maximum fluorescence intensity ($\Delta F_{max}/F_o$). Experimental error represents ± 2 S.D. Competitive equilibrium binding studies and data analysis were performed as described under "Experimental procedures."

SC(1–246) mutants	KC	K_D from ProT^{QQQ} activation	V_{lim}	$\Delta F_{max}/Fo$	ΔG
	nM	*nM*			*kcal/mol*
I1I2V3	4 ± 3	3 ± 1	0.80 ± 0.03	0.57 ± 0.01	−11.51
R1H2W3	35 ± 23	124 ± 48	0.31 ± 0.03	0.58 ± 0.01	−10.16
F1L2Q3	39 ± 25	> 500	0.06 ± 0.05	0.58 ± 0.01	−10.11
E1L2K3	42 ± 27	309 ± 54	0.26 ± 0.01	0.58 ± 0.01	−10.07
E1S2W3	48 ± 32	28 ± 42	0.03 ± 0.01	0.58 ± 0.01	−9.98
G1G2G3	48 ± 33	29 ± 20	0.11 ± 0.01	0.58 ± 0.01	−9.98
D1D2Y3	55 ± 36	545 ± 145	0.19 ± 0.03	0.58 ± 0.01	−9.90

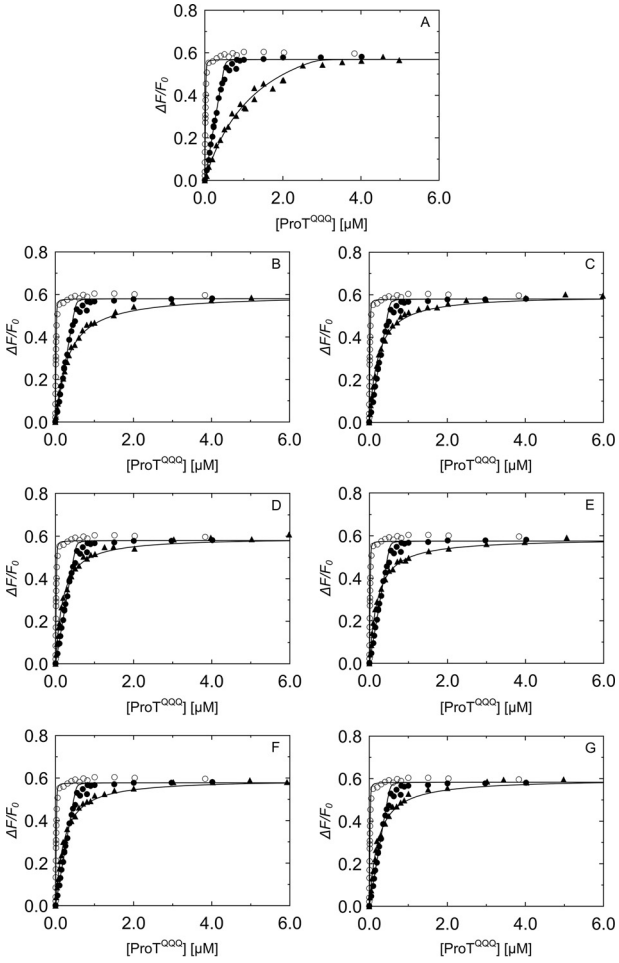

Figure 7. Competitive binding titrations of SC(1–246) N-terminal triple mutants with ProT^{QQQ}. Titrations of the probe, SC(1–246)-BODIPY (29 nM (○) and 502 nM (●)) with ProT^{QQQ} from Fig. 4 served as reference curves for competitive titrations of SC(1–246) mutants. The probe concentration for all of the competitive titrations (▲) in *A–G* was 50 nM. Concentrations of competing SC(1–246) mutants were as follows: I1I2V3 2.84 μM (*A*), R1H2W3 7.59 μM (*B*), F1L2Q3 5.49 μM (*C*), E1S2W3 5.74 μM (*D*), D1D2Y3 7.65 μM (*E*), E1L2K3 5.77 μM (*F*), and G1G2G3 6.44 μM (*G*). Titrations of probe and competitor were simultaneously analyzed by the cubic binding equation to obtain K_C, stoichiometry, and maximum fluorescence intensity ($\Delta F_{max}/F_o$) of the SC(1–246) mutants (Table 4).

eration of the Pre2 active site in the complex (19). Based on the ability to clot plasma, SC variants from different *S. aureus* strains are classified into 12 different serotypes (27, 28). The SC D1 domain (except for the first seven residues) and the D2 domain of 10 different *S. aureus* serotypes showed identities ranging from 53 to 89% (D1) and from 57 to 92% (D2), with the conservation of predicted ProT residues (29). A new classification scheme, based on the D1 domain of SC from 103 *S. aureus* strains, showed an average of 67.1% D1 domain identity among the 12 SC serotypes, with the first seven N-terminal residues being highly conserved (28). Our studies showed that the conserved I1V2 residues in the natural N terminus of SC(1–325) were required for ProT activation, with SC(2–325) being 6-fold less efficient and SC(3–325) only exhibiting <2% activity. However, a Met-SC(1–325) construct still containing the initiating Met residue (Met^1-Ile^2-Val^3) also showed ProT activation potency and binding with K_D = 17 ± 2 nM, suggesting some degree of SC promiscuity and also flexibility of the ProT Ile^{16} pocket in accommodating different residues (19). The first six N-terminal SC residues were fully resolved in the structure of the SC(1–325)·Pre2 complex, and modeling showed that extending or shortening this hexapeptide by one residue still allowed for interaction with the prothrombin 2 activation pocket. Also, von Willebrand factor–binding protein (vWbp), a nonproteolytic ProT activator from *S. aureus* Tager 104 Newman D2, and streptokinase, a nonproteolytic plasminogen activator from *Streptococcus equisimilis* and *Streptococcus pyogenes*, have N-terminal I1V2 and I1A2 sequences, respectively, suggesting that the Ile^{16} pocket of serine protease zymogens is highly suited to accommodate small nonpolar residues. Hence, we wanted to examine the tolerance of the Ile^{16} pocket of ProT for a panel of N-terminal residues. This could help decipher why SC has this unique N-terminal conservation and predict whether under selective pressure, *S. aureus* may be capable of producing SC variants with other N-terminal residues that could have affinity and potency similar or superior to that of SC with the canonical I1V2 residues.

Our previous studies reported that SC(1–325) binds to ProT with K_D 0.3 ± 0.2 nM (19). The extremely high affinity makes this construct less suitable for use as a probe in measuring competitive binding of SC mutants with weaker affinity. Therefore, we used truncated SC(1–246) with a S7C substitution for BODIPY labeling, which we characterized to have a K_D of ~3 nM for ProT^{QQQ} binding, a minimally weaker interaction than what we measured for competitive binding of WT SC(1–246) with K_D of ~1 nM, due to introduction of the fluorescence label. This probe allowed measurement of affinities of competitive N-terminal mutants up to K_D ~650 nM. SC(1–246) contains an

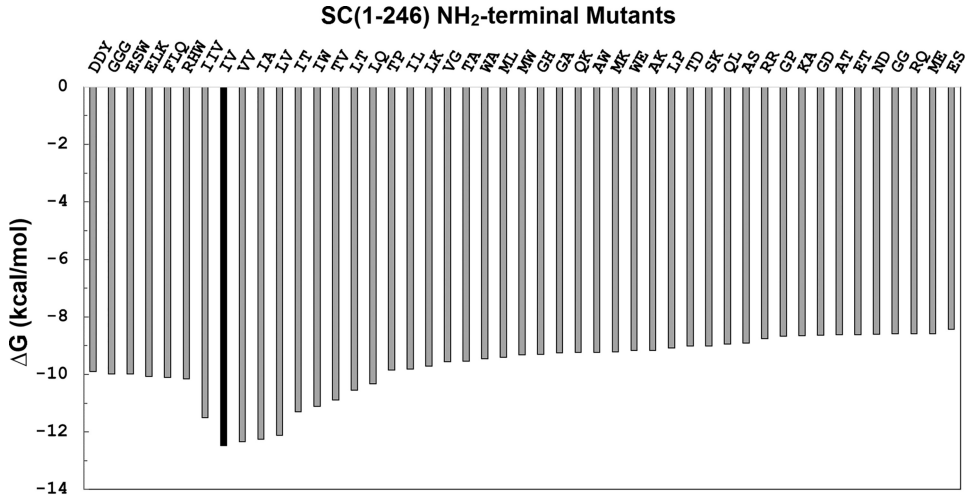

Figure 8. Gibbs free energy of the SC(1–246) N-terminal double and triple mutants for binding to ProT^{QQQ}. ΔG values were calculated using K_D values obtained from equilibrium binding, as described under "Experimental Procedures."

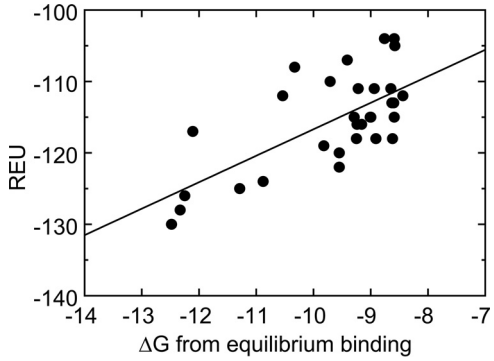

Figure 9. Correlation between REU and ΔG values calculated from equilibrium binding.

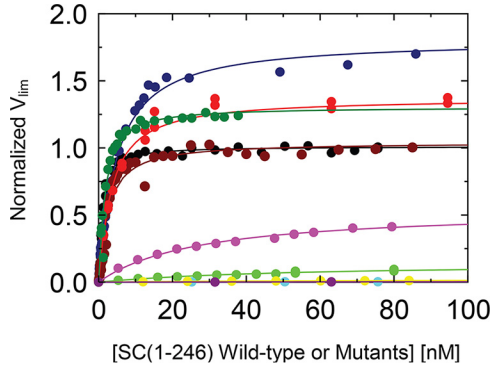

Figure 10. Activation of ProT^{QQQ} by SC(1–246) WT or double mutants. ProT^{QQQ} (1, 10, or 20 nM) and SC(1–246) WT (*black circles*) and a representative selection of mutants (*navy blue*, I1A2; *red*, L1T2; *dark green*, L1Q2; *brown*, V1V2; *purple*, A1K2; *green*, A1W2; *cyan*, K1A2; *yellow*, Q1K2; *eggplant*, E1S2) were incubated for 10 min at 25 °C, and the reaction was initiated by adding S-2238. Activation of ProT^{QQQ} was measured by the relative rates of increase in absorbance at 405 nm, and weak-binding mutants with low activation potency were titrated up to 1300 nM. The data were analyzed as described under "Experimental Procedures."

intact D1 domain but lacks residues 247–282 of the (pro)-thrombin (pro)exosite I-binding D2 domain, which is thought to result in weakened affinity compared with a construct with an intact D2 domain.

The mutants in this study can be categorized in four groups with regard to ProT^{QQQ} binding and activation, compared with WT SC(1–246): (*a*) similar affinity, and similar or increased activation potency, in constructs with conserved or homologous nonpolar N-terminal residues; (*b*) modestly to significantly weaker equilibrium binding affinity, but substrate-induced, tight K_D and induced fit to the Ile^{16} pocket, and similar or increased activation potency; (*c*) modestly weaker affinity but significantly reduced activation potency due to poor fit of the N-terminal residues and mainly governed by partial D2 binding; and (*d*) significantly weaker affinity and significantly reduced or abolished activation potency in constructs with polar or proline-containing N termini, perhaps by triggering unfavorable long-range binding interactions through electrostatic or steric conformational changes. The overall affinity of our constructs for ProT^{QQQ} is proposed to result from the combined effects of binding of N-terminal SC(1–246) residues to the ProT^{QQQ} Ile^{16} pocket, contact of the D1 domain with the ProT^{QQQ} 148-loop, and binding of the truncated D2 domain to ProT proexosite I, whereas the activation potency is critically defined by the capacity of SC(1–246) residue 1 forming a salt bridge with ProT^{QQQ} Asp^{194} and an adequate and, if necessary, substrate-inducible fit of residue 2 in the ordered Ile^{16} pocket. Our previous studies indicated that isolated D1 bound to ProT with modest affinity, K_D ~780 nM when measured by ProT activation and K_D ~3.5 μM when measured by fluorescence equilibrium binding in the absence of a substrate. Isolated D2 binding to ProT proexosite I did not cause ProT activation due to the absence of the critical N-terminal residues; however, its affinity by equilibrium binding was ~30 nM (19, 30).

Active-site ligands with high affinity for the proteinase are known to induce a proteinase-like conformation in the zymogen. Occupation of the ProT^{QQQ} specificity site by a thrombin substrate caused a ~5-fold allosteric tightening of the D1 binding, which is facilitated by favorable steric complementarity of the first two N-terminal residues of SC and the Ile^{16}-binding pocket (Fig. 11). A similar allosteric modulation is caused by binding of the *S. aureus*-secreted vWbp to prothrombin derivatives, with tighter binding to prothrombin forms that have their active site labeled with D-Phe-Pro-Arg-chloromethylketone (22). This tightening effect was previously also observed

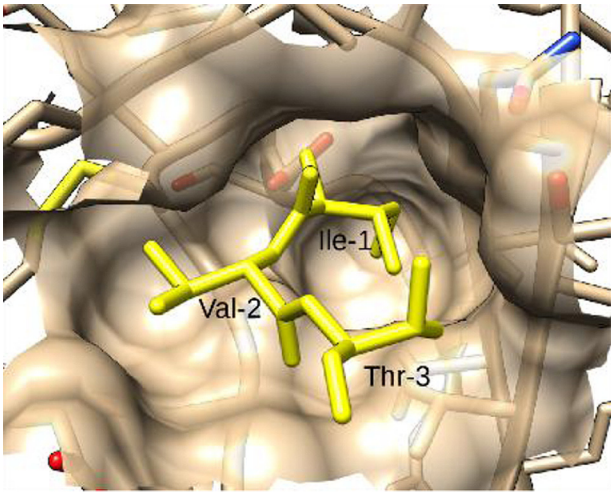

Figure 11. Binding site complementarity between SC(1–325) and prethrombin 2. Native residues I1V2T3 of SC are shown in the Ile^{16} pocket of prothrombin 2. The steric complementarity excludes the possibility of adding additional bulk to the N terminus of SC without generating energetically unfavorable clashes with neighboring residues.

for binding of small peptides in the Ile^{16} pocket of trypsinogen with its specificity site occupied by pancreatic trypsin inhibitor (PTI) or covalently bound *p*-guanidinobenzoate (*p*GB) (23, 31). In the presence of PTI or *p*GB, the Ile^{16} pocket is fully formed, in contrast with free trypsinogen, which shows a disordered specificity pocket and Ile^{16}-binding pocket in the crystal structure. We found that the V1V2, I1A2, and L1V2 double mutants of SC(1–246) bind $ProT^{QQQ}$ with similar affinities and show similar or higher potency in activating $ProT^{QQQ}$, and the I1I2V3 triple mutant binds and activates $ProT^{QQQ}$ only slightly more weakly. In a study with isolated di- and oligopeptides, Bode (23) reported that the more effective peptides I1V2 and I1V2G3 used in activation studies of trypsinogen carrying a ligand in the specificity pocket (*p*GB or pancreatic trypsin inhibitor) were identical to the newly formed N-terminal sequence after cleavage of the activation peptide. However, the peptides V1V2, I1A2, and L1V2 bound to *p*GB-trypsinogen with affinities 30-, 160-, and 190-fold weaker than I1V2, respectively. In our studies, additional interactions of the D1 and the truncated D2 domains were shown to contribute to enhanced binding affinity and $ProT^{QQQ}$ activation potential by SC(1–246) mutants with these N-terminal sequences. In the I1I2V3 triple mutant, Ile^2 is similar in size and hydrophobicity to Val^2 of the WT construct. Consequently, there was not much reduction in $ProT^{QQQ}$ affinity and activation potency of this mutant. The equilibrium binding and kinetic data presented here indicate that small and nonpolar residues are preferred over bulky and charged ones for sufficient ProT binding and activation (Table 2), due to a better fit in the Ile^{16} pocket, even in the disordered state. The Val^1, Leu^1, and Ala^2 residues of the double mutants are as functional as Ile^1 and Val^2 of WT SC(1–246). The presence of these residues in the pocket favors the packing and alignment of the side chains triggering conformational activation in a similar fashion as seen in the SC(1–325)·Pre2 complex, with the α-ammonium group of Val^1 possibly connecting through a salt bridge with Asp^{194}. Ala^2 may be stabilized through the formation of a hydrogen bond with Asp^{189} in the $ProT^{QQQ}$ specificity pocket, as observed for Val^2 in the SC(1–325)·Pre2 crystal structure. In the crystal structure of SC(1–325)·Pre2, Ile^1 is completely buried in the hydrophobic Ile^{16} pocket, whereas Val^2 partially contacts the outer solvent. Replacement of valine with the bulky amino acid leucine showed a 15-fold decrease in affinity for pGB-trypsinogen (23). Even though binding and insertion of the first two N-terminal are additive, the Ile^{16} pocket can accommodate a less favorable residue at the second position.

Interestingly, the T1A2 mutant has the same T1A2T3 residues as those proteolytically generated in a ProT mutant upon cleavage at Arg^{320} (32). Substitution of IVE to TAT following ProT Arg^{320} did not prevent cleavage but ultimately generated a thrombin mutant IIa_{TAT} with zymogen-like properties that bound the active site probe DAPA with ~32,000-fold weaker affinity than WT thrombin (K_D ~1 nM) and only had 0.2% specific activity toward the thrombin-specific chromogenic substrate S2238. Our T1A2 mutant bound $ProT^{QQQ}$ with equilibrium K_D of 100 ± 27 nM, and 5.2 ± 0.2 nM from ProT activation, in the presence of a chromogenic substrate and an activation potential 1.3 times that of WT SC(1–246). This functional mutant may attribute its potential of salt bridge formation with $ProT^{QQQ}$ Asp^{194} and zymogen activation to cumulative N-terminal, D1 and D2 conformational interactions that shift the zymogen–protease equilibrium in IIa_{TAT} toward the protease conformation.

Equilibrium binding of various mutants involving Pro and Trp was moderate to weak (T1P2, M1W2, A1W2, and L1P2, ~60–200 nM), and their dramatically reduced activation potency suggests nonproductive interaction with the Ile^{16} pocket and binding through the partial D2 domain that may be perturbed by electrostatic or steric effects introduced by the mutations. Variations in the structural orientation of the partial D2 domain may alter binding and lead to weaker overall mutant affinity for $ProT^{QQQ}$. Typically, these mutants were outliers in the correlation of predicted REU scores and measured ΔG values of equilibrium binding (Fig. S1), suggesting that the sampling protocol employed was not sufficient to overcome the major structural perturbation required to insert the steric bulk of a Trp residue or to accommodate the backbone angle restriction imposed by a Pro residue. The high energy penalty can be interpreted as a clear signal that the new sequence is incompatible with the native structure. Triple mutants containing bulky aromatic or charged residues as well as G1G2G3 bound ~10-fold tighter than the G1G2 double mutant with K_D of 48 ± 33 nM, respectively, suggesting that Gly at position 3 instead of native Thr is more conducive to steric complementarity. However, the low activation potencies of both the double and triple mutant indicated impaired salt bridge formation with $ProT^{QQQ}$ Asp^{194}.

In conclusion, we have determined the affinities of a panel of 46 different SC N-terminal mutants for $ProT^{QQQ}$ and showed that the Ile^{16} pocket is specific for accommodating residues that are similar in size to I1V2, but improved fit for a variety of preferably noncharged position 2 residues except for proline can be induced by small substrate binding. This characterization of the SC N-terminal residues in the SC-ProT complex provides further information to better design antibodies as

drugs to target the SC N terminus. Our results suggest the distinct possibility that *S. aureus* may be capable of adapting to continuous use of antibiotics and selection pressure to escape the human immune response, by generating SC variants with similar or higher efficiency to activate ProT.

Experimental procedures

Expression, purification, and labeling of proteins

SC(1–246) was cloned into a modified pET30b(+) vector (Novagen) containing an N-terminal His_6 tag followed by a tobacco etch virus cleavage site (19, 30). The SC(1–246) N-terminal mutants were prepared through site-directed mutagenesis using degenerate and specific primers (Table S1), and mutations were confirmed by DNA sequencing. The mutants were expressed in Rosetta 2 (DE3) pLysS *Escherichia coli* in the presence of 100 μg/ml kanamycin, and expression was induced by 10 mg/ml lactose for 4 h. Mutants were purified from inclusion bodies, and the His_6 tag was removed as described (33, 34). The proteins were stored in 50 mM HEPES, 125 mM NaCl, pH 7.4, at −80 °C until use. The mutant concentrations were determined using the extinction coefficients and molecular mass calculated by the Expasy tool, RRID:SCR_018087 (Table S2). HEK293 cells expressing $ProT^{QQQ}$, in which the prothrombinase cleavage site Arg^{271} and the thrombin cleavage sites Arg^{155} and Arg^{284} were replaced by glutamine to prevent degradation, were a gift from Dr. Sriram Krishnaswamy (University of Pennsylvania School of Medicine) (20). $ProT^{QQQ}$ was expressed, purified, and stored as described (35, 36). Four separate $ProT^{QQQ}$ batches were prepared, and the concentrations were determined using $E_{280\ nm,0.1\%}$ 1.47 ml mg^{-1} cm^{-1} and M_r 72,000.

Preparation and characterization of SC(1–246)-BODIPY

To create a labeled SC construct, Ser^7 of SC(1–246) was converted to cysteine through site-directed mutagenesis (Agilent Technologies) and confirmed by DNA sequencing. Purified SC(1–246)-S7C was reduced with 2 mM DTT and dialyzed against 5 mM MES, 125 mM NaCl, 2 mM DTT, pH 6.0. The reduced protein was run on Sephadex G-25 (1 × 25 cm) in 50 mM HEPES, 125 mM NaCl, 1 mg/ml PEG, 10 mM EDTA, pH 7.4, buffer to remove free DTT. Approximately 5–10 mg of protein was incubated for 1 h at 25 °C with a 10-fold molar excess of BODIPY-FL-iodoacetamide (Thermo Fisher Scientific) to label the free S7C thiol. The excess probe was removed by Sephadex G-25 chromatography in 50 mM HEPES, 125 mM NaCl, 0.1 mM EDTA, pH 7.4, buffer. Labeled SC(1–246)-S7C-BODIPY-FL (SC(1–246)-BODIPY) was dialyzed against storage buffer (50 mM HEPES, 125 mM NaCl, pH 7.4) and stored at −80 °C. The concentration and labeling ratio were determined using $E_{280\ nm,\ 0.1\%}$ 0.936 ml mg^{-1} cm^{-1} and M_r 29,150 for WT SC(1–246) and SC(1–246)-S7C, and $E_{505\ nm}$ of 63,771 cm^{-1} M^{-1} for BODIPY-FL-iodoacetamide. An absorbance ratio ($A_{280\ nm}$/$A_{505\ nm}$) of 0.03 was used to correct for the probe contribution to absorbance at 280 nm. The purity of SC(1–246)-BODIPY was established by 4–20% polyacrylamide SDS-PAGE under reduced and nonreduced conditions. The fluorescence of the labeled protein was imaged under UV light, and proteins were then stained with colloidal Coomassie Blue G-250. To determine whether SC(1–246)-BODIPY forms a binary complex with $ProT^{QQQ}$, a fixed concentration (2.5 μM) of $ProT^{QQQ}$ was incubated with different concentrations of SC(1–246)-BODIPY (0, 0.5, 1.0, and 1.5 μM) at 25 °C for 15–30 min. The samples were run on a 6% polyacrylamide gel under native conditions (Tris-glycine buffer, pH 8.3, no SDS) at 4 °C. The fluorescence was imaged, and the proteins were stained as described above.

Prothrombin activation assay

Activity titrations of ProT complexes with WT or mutant SC(1–246) were performed in 50 mM HEPES, 110 mM NaCl, 5 mM $CaCl_2$, 1 mg/ml PEG 8000, pH 7.4, buffer, in PEG 20,000-coated 96-well plates (Nunc). Varying concentrations of WT or mutant SC(1–246) were incubated with 1, 10, or 20 nM ProT for 10 min at 25 °C. The reaction was initiated by the addition of 600 μM chromogenic substrate S-2238 (Diapharma), and the rate was measured in a ThermoMax plate reader (Thermo Fisher Scientific) for 10 min at 405 nm until the absorbance reached 0.1. Initial rates (mAbs/min) for the mutants were normalized to that of WT SC(1–246). The normalized rate dependences as a function of the SC(1–246) concentration were fitted by the quadratic binding equation using SCIENTIST (MicroMath) to obtain the V_{lim} and K_D (19).

Direct and competitive fluorescence equilibrium binding

Fluorescence measurements were performed with a PTI QuantaMaster 30 spectrofluorometer at 25 °C using acrylic cuvettes coated with PEG 20,000. Titrations were performed in 50 mM HEPES, 110 mM NaCl, 5 mM $CaCl_2$, 1 mg/ml PEG 8000, pH 7.4, buffer with 1 mg/ml ovalbumin, and fluorescence was measured at λ_{ex} = 496 nm (3–6-nm band pass) and λ_{em} = 535 nm (4–6-nm band pass). Two fixed concentrations of SC(1–246)-BODIPY were titrated with the ligand, $ProT^{QQQ}$. The competitive binding assays were performed with one fixed concentration of SC(1–246)-BODIPY in the presence of a single fixed concentration of unlabeled WT or mutant SC(1–246) competitor, titrated with the ligand, $ProT^{QQQ}$. The SC(1–246)-BODIPY control titrations with $ProT^{QQQ}$ were performed to obtain the stoichiometry and K_O for SC(1–246)-BODIPY. The titrations of SC(1–246)-BODIPY in the presence of competing WT or mutant SC(1–246) were performed to obtain the stoichiometry and dissociation constant K_C for the competitors. The fractional change in fluorescence was calculated as $(F_{obs} - F_o)/F_o = \Delta F/F_o$, and the data were fit by the quadratic binding equation (37) using SCIENTIST (MicroMath) software. For the competition experiments, titrations in the absence and presence of competitor were fit simultaneously by the cubic binding equation (37). Nonlinear least-squares fitting was performed using SCIENTIST (MicroMath) either with or without fixed stoichiometry for the competitive data to obtain the dissociation constants K_O and K_C, maximum fluorescence intensities ($(F_{max} - F_o)/F_o = \Delta F_{max}/F_o$), and stoichiometric factors n for SC(1–246)-BODIPY and m for unlabeled WT and mutant SC(1–246). The error estimates represent the 95% confidence interval. The Gibbs free energy (ΔG) values for WT and mutant SC(1–246) binding to $ProT^{QQQ}$ were calculated using the equation, $\Delta G = RT \ln K_D$, where $R = 1.987 \times 10^{-3}$ kcal mol^{-1} $degree^{-1}$ and T = 298.15 K (25 °C), and K_D is expressed in M.

Computational modeling

To analyze the energetic effects of the N-terminal mutations of SC(1–246) on the binding with ProT^{QQQ}, the mutations were performed *in silico* using the Rosetta software suite (RRID: SCR_015701) (38). The X-ray crystal structure of the complex 1nu9 (19) was relaxed using Rosetta3 (August 2016 build 58479), using constraints to maintain atomic positions close to the experimental input structure. The relaxation was performed 100 times, and the lowest-energy structure was selected for mutation (/rosetta-3.9/main/source/bin/relax.default.linuxgccrelease -s 1nu9_cleaned.pdb -in:file:fullatom -nstruct 100 -relax:fast -relax:constrain_relax_to_start_coords). Mutations were introduced into the structure using Rosetta's fixed backbone design (fixbb) application (39) and a resfile specifying the identities of residues at positions 1, 2, and 3. All 20 amino acids were tested at each of the three positions, resulting in 8,000 output structures, representing putative single, double, and triple mutants (/rosetta-3.9/main/source/bin/fixbb.default.linuxgccrelease -s relaxed_with_constraints.pdb -resfile resfiles/$key -in:file:fullatom -use_input_sc -ex1 -ex2 -out:path:pdb pdbfiles -out:path:score scorefiles). The predicted change in the interaction energy between the mutated SC(1–246) and Pre-2 was calculated using Rosetta's interface analyzer application, to evaluate the resulting changes in the energetic binding contribution of the N-terminal segment of SC(1–246). (/rosetta-3.9/main/source/bin/InterfaceAnalyzer.default.linuxgccrelease -in:path ../pdbfiles -in:file:l structure_batch.list -add_regular_scores_to_scorefile -out:path:pdb pdbfiles -out:path:score scorefiles -out:file:scorefile structure_batch.fasc), and the sixth column "dG_separated" was extracted using awk. (% cat ../scorefiles/*.fasc | awk '{print $NF " " $6}' | grep -v SEQUENCE | grep -v description | sort -nrk2 > sorted_interface_energies.list).

Data availability

The structure of the SC(1–325)·Pre2 complex 1NU9 is available in the Protein Data Bank. All remaining data are contained within the article and supporting information.

Author contributions—A. A. M., H. K. K., M. E. A., B. H. G., J. H. S., J. M., P. E. B., and I. M. V. data curation; A. A. M., H. K. K., M. E. A., B. H. G., and J. M. formal analysis; A. A. M., H. K. K., M. E. A., and P. P. investigation; A. A. M., H. K. K., M. E. A., B. H. G., P. P., J. H. S., and P. E. B. methodology; A. A. M. and H. K. K. writing-original draft; H. K. K., P. P., P. E. B., and I. M. V. conceptualization; P. P. and I. M. V. writing-review and editing; J. H. S. and J. M. software; J. H. S. and J. M. validation; P. E. B. and I. M. V. supervision; P. E. B. and I. M. V. funding acquisition; P. E. B. and I. M. V. project administration.

References

1. Klein, E., Smith, D. L., and Laxminarayan, R. (2007) Hospitalizations and deaths caused by methicillin-resistant *Staphylococcus aureus*, United States, 1999–2005. *Emerg. Infect. Dis.* **13,** 1840–1846 CrossRef Medline
2. McGavin, M. J., and Heinrichs, D. E. (2012) The staphylococci and staphylococcal pathogenesis. *Front. Cell Infect. Microbiol.* **2,** 66 CrossRef Medline
3. Lowy, F. D. (1998) *Staphylococcus aureus* infections. *N. Engl. J. Med.* **339,** 520–532 CrossRef Medline
4. Hartleib, J., Köhler, N., Dickinson, R. B., Chhatwal, G. S., Sixma, J. J., Hartford, O. M., Foster, T. J., Peters, G., Kehrel, B. E., and Herrmann, M. (2000) Protein A is the von Willebrand factor binding protein on *Staphylococcus aureus*. *Blood* **96,** 2149–2156 Medline
5. Herrmann, M., Suchard, S. J., Boxer, L. A., Waldvogel, F. A., and Lew, P. D. (1991) Thrombospondin binds to *Staphylococcus aureus* and promotes staphylococcal adherence to surfaces. *Infect. Immun.* **59,** 279–288 CrossRef Medline
6. Herrmann, M., Lai, Q. J., Albrecht, R. M., Mosher, D. F., and Proctor, R. A. (1993) Adhesion of *Staphylococcus aureus* to surface-bound platelets: role of fibrinogen/fibrin and platelet integrins. *J. Infect. Dis.* **167,** 312–322 CrossRef Medline
7. Kuypers, J. M., and Proctor, R. A. (1989) Reduced adherence to traumatized rat heart valves by a low-fibronectin-binding mutant of *Staphylococcus aureus*. *Infect. Immun.* **57,** 2306–2312 CrossRef Medline
8. Moreillon, P., Entenza, J. M., Francioli, P., McDevitt, D., Foster, T. J., François, P., and Vaudaux, P. (1995) Role of *Staphylococcus aureus* coagulase and clumping factor in pathogenesis of experimental endocarditis. *Infect. Immun.* **63,** 4738–4743 CrossRef Medline
9. Patti, J. M., Allen, B. L., McGavin, M. J., and Höök, M. (1994) MSCRAMM-mediated adherence of microorganisms to host tissues. *Annu. Rev. Microbiol.* **48,** 585–617 CrossRef Medline
10. Que, Y. A., François, P., Haefliger, J. A., Entenza, J. M., Vaudaux, P., and Moreillon, P. (2001) Reassessing the role of *Staphylococcus aureus* clumping factor and fibronectin-binding protein by expression in *Lactococcus lactis*. *Infect. Immun.* **69,** 6296–6302 CrossRef Medline
11. Siboo, I. R., Cheung, A. L., Bayer, A. S., and Sullam, P. M. (2001) Clumping factor A mediates binding of *Staphylococcus aureus* to human platelets. *Infect. Immun.* **69,** 3120–3127 CrossRef Medline
12. McAdow, M., Missiakas, D. M., and Schneewind, O. (2012) *Staphylococcus aureus* secretes coagulase and von Willebrand factor binding protein to modify the coagulation cascade and establish host infections. *J. Innate Immun.* **4,** 141–148 CrossRef Medline
13. Cabell, C. H., Jollis, J. G., Peterson, G. E., Corey, G. R., Anderson, D. J., Sexton, D. J., Woods, C. W., Reller, L. B., Ryan, T., and Fowler, V. G., Jr. (2002) Changing patient characteristics and the effect on mortality in endocarditis. *Arch. Intern. Med.* **162,** 90–94 CrossRef Medline
14. Soulier, J. P., and Prou-Wartelle, O. (1967) Study of thrombin-coagulase. *Thromb. Diath. Haemorrh.* **17,** 321–334 Medline
15. Kawabata, S., Morita, T., Iwanaga, S., and Igarashi, H. (1985) Difference in enzymatic properties between α-thrombin-staphylocoagulase complex and free α-thrombin. *J. Biochem.* **97,** 1073–1078 CrossRef Medline
16. Kawabata, S., Miyata, T., Morita, T., Miyata, T., Iwanaga, S., and Igarashi, H. (1986) The amino acid sequence of the procoagulant- and prothrombin-binding domain isolated from staphylocoagulase. *J. Biol. Chem.* **261,** 527–531 Medline
17. Kawabata, S., and Iwanaga, S. (1994) Structure and function of staphylothrombin. *Semin. Thromb. Hemost.* **20,** 345–350 CrossRef Medline
18. Panizzi, P., Friedrich, R., Fuentes-Prior, P., Bode, W., and Bock, P. E. (2004) The staphylocoagulase family of zymogen activator and adhesion proteins. *Cell Mol. Life Sci.* **61,** 2793–2798 CrossRef Medline
19. Friedrich, R., Panizzi, P., Fuentes-Prior, P., Richter, K., Verhamme, I., Anderson, P. J., Kawabata, S., Huber, R., Bode, W., and Bock, P. E. (2003) Staphylocoagulase is a prototype for the mechanism of cofactor-induced zymogen activation. *Nature* **425,** 535–539 CrossRef Medline
20. Kamath, P., and Krishnaswamy, S. (2008) Fate of membrane-bound reactants and products during the activation of human prothrombin by prothrombinase. *J. Biol. Chem.* **283,** 30164–30173 CrossRef Medline
21. Kellogg, E. H., Leaver-Fay, A., and Baker, D. (2011) Role of conformational sampling in computing mutation-induced changes in protein structure and stability. *Proteins* **79,** 830–838 CrossRef Medline
22. Kroh, H. K., and Bock, P. E. (2012) Effect of zymogen domains and active site occupation on activation of prothrombin by von Willebrand factor-binding protein. *J. Biol. Chem.* **287,** 39149–39157 CrossRef Medline
23. Bode, W. (1979) The transition of bovine trypsinogen to a trypsin-like state upon strong ligand binding. II. The binding of the pancreatic trypsin inhibitor and of isoleucine-valine and of sequentially related peptides to trypsinogen and to *p*-guanidinobenzoate-trypsinogen. *J. Mol. Biol.* **127,** 357–374 CrossRef Medline

24. Krishnaswamy, S. (2013) The transition of prothrombin to thrombin. *J. Thromb. Haemost.* **11,** 265–276 CrossRef Medline
25. Bode, W., and Huber, R. (1978) Crystal structure analysis and refinement of two variants of trigonal trypsinogen: trigonal trypsin and PEG (polyethylene glycol) trypsinogen and their comparison with orthorhombic trypsin and trigonal trypsinogen. *FEBS Lett.* **90,** 265–269 CrossRef Medline
26. Khan, A. R., and James, M. N. (1998) Molecular mechanisms for the conversion of zymogens to active proteolytic enzymes. *Protein Sci.* **7,** 815–836 CrossRef Medline
27. Watanabe, S., Ito, T., Sasaki, T., Li, S., Uchiyama, I., Kishii, K., Kikuchi, K., Skov, R. L., and Hiramatsu, K. (2009) Genetic diversity of staphylocoagulase genes (coa): insight into the evolution of variable chromosomal virulence factors in *Staphylococcus aureus*. *PLoS ONE* **4,** e5714 CrossRef Medline
28. Kanemitsu, K., Yamamoto, H., Takemura, H., Kaku, M., and Shimada, J. (2001) Relatedness between the coagulase gene 3′-end region and coagulase serotypes among *Staphylococcus aureus* strains. *Microbiol. Immunol.* **45,** 23–27 CrossRef Medline
29. Watanabe, S., Ito, T., Takeuchi, F., Endo, M., Okuno, E., and Hiramatsu, K. (2005) Structural comparison of ten serotypes of staphylocoagulases in *Staphylococcus aureus*. *J. Bacteriol.* **187,** 3698–3707 CrossRef Medline
30. Panizzi, P., Friedrich, R., Fuentes-Prior, P., Kroh, H. K., Briggs, J., Tans, G., Bode, W., and Bock, P. E. (2006) Novel fluorescent prothrombin analogs as probes of staphylocoagulase-prothrombin interactions. *J. Biol. Chem.* **281,** 1169–1178 CrossRef Medline
31. Bode, W., and Huber, R. (1976) Induction of the bovine trypsinogen-trypsin transition by peptides sequentially similar to the N-terminus of trypsin. *FEBS Lett.* **68,** 231–236 CrossRef Medline
32. Bianchini, E. P., Orcutt, S. J., Panizzi, P., Bock, P. E., and Krishnaswamy, S. (2005) Ratcheting of the substrate from the zymogen to proteinase conformations directs the sequential cleavage of prothrombin by prothrombinase. *Proc. Natl. Acad. Sci. U.S.A.* **102,** 10099–10104 CrossRef Medline
33. Kroh, H. K., Panizzi, P., and Bock, P. E. (2009) Von Willebrand factor-binding protein is a hysteretic conformational activator of prothrombin. *Proc. Natl. Acad. Sci. U.S.A.* **106,** 7786–7791 CrossRef Medline
34. Panizzi, P., Boxrud, P. D., Verhamme, I. M., and Bock, P. E. (2006) Binding of the COOH-terminal lysine residue of streptokinase to plasmin(ogen) kringles enhances formation of the streptokinase.plasmin(ogen) catalytic complexes. *J. Biol. Chem.* **281,** 26774–26778 CrossRef Medline
35. Orcutt, S. J., and Krishnaswamy, S. (2004) Binding of substrate in two conformations to human prothrombinase drives consecutive cleavage at two sites in prothrombin. *J. Biol. Chem.* **279,** 54927–54936 CrossRef Medline
36. Newell-Caito, J. L., Laha, M., Tharp, A. C., Creamer, J. I., Xu, H., Maddur, A. A., Tans, G., and Bock, P. E. (2011) Notecarin D binds human factor V and factor Va with high affinity in the absence of membranes. *J. Biol. Chem.* **286,** 38286–38297 CrossRef Medline
37. Bock, P. E., Olson, S. T., and Björk, I. (1997) Inactivation of thrombin by antithrombin is accompanied by inactivation of regulatory exosite I. *J. Biol. Chem.* **272,** 19837–19845 CrossRef Medline
38. Leaver-Fay, A., Tyka, M., Lewis, S. M., Lange, O. F., Thompson, J., Jacak, R., Kaufman, K., Renfrew, P. D., Smith, C. A., Sheffler, W., Davis, I. W., Cooper, S., Treuille, A., Mandell, D. J., Richter, F., *et al.* (2011) ROSETTA3: an object-oriented software suite for the simulation and design of macromolecules. *Methods Enzymol.* **487,** 545–574 CrossRef Medline
39. Kuhlman, B., Dantas, G., Ireton, G. C., Varani, G., Stoddard, B. L., and Baker, D. (2003) Design of a novel globular protein fold with atomic-level accuracy. *Science* **302,** 1364–1368 CrossRef Medline